# INTERNATIONAL SOCIETY FOR SOIL MECHANICS AND GEOTECHNICAL ENGINEERING



This paper was downloaded from the Online Library of the International Society for Soil Mechanics and Geotechnical Engineering (ISSMGE). The library is available here:

# https://www.issmge.org/publications/online-library

This is an open-access database that archives thousands of papers published under the Auspices of the ISSMGE and maintained by the Innovation and Development Committee of ISSMGE.

The paper was published in the proceedings of the 20<sup>th</sup> International Conference on Soil Mechanics and Geotechnical Engineering and was edited by Mizanur Rahman and Mark Jaksa. The conference was held from May 1<sup>st</sup> to May 5<sup>th</sup> 2022 in Sydney, Australia.

# Evaluation of residual strength of rocks based on acoustic emission data using Al

Évaluation de la résistance résiduelle des roches sur la base des données d'émission acoustique à l'aide de l'IA

# **Negin Yousefpour**

Infrastructure Engineering Department, The University of Melbourne, Australia, negin.yousefpour@unimelb.edu.au

#### Mehdi Pouragha

Civil and Environmental Engineering Department, Carleton University, Canada

ABSTRACT: Acoustic emission (AE) is one of the most common sensing methods for monitoring the behaviour of brittle materials such as rock and concrete. This study uses Discrete Element Method (DEM) simulations to correlate the pre-failure AE data to the post-failure characteristics such as residual strength. The deep learning method using the Long Short-Term Memory algorithm (LSTM) has been adopted to learn from the data set created via parametric DEM simulations. Various configurations of the LSTM algorithm were trained considering multiple combinations of input features, i.e. strain, stress and AE energy records. The prim AI models have shown promising accuracy in prediction of residual strength decay with strain, based on patterns in AE energy records. The results indicate that the pre-failure AE energy patterns indeed encapsulate information about the developing failure mechanisms and the post-failure response, which can be captured by Artificial Intelligence.

RÉSUMÉ: L'émission acoustique (AE) fait partie des mesures les plus pratiques pour surveiller le comportement des matériaux fragiles tels que la roche et le béton. Cette étude utilise des simulations de la méthode des éléments discrets (DEM) pour corréler les données AE prédéfaillance aux caractéristiques postrupture telles que la résistance résiduelle. La méthode d'apprentissage en profondeur utilisant l'algorithme de mémoire à long terme (LSTM) a été adoptée pour apprendre à partir de l'ensemble de données créé via des simulations DEM paramétriques. Diverses configurations de l'algorithme LSTM ont été entraînées en tenant compte de multiples combinaisons de caractéristiques d'entrée, c'estàdire des enregistrements d'énergie de déformation, de contrainte et d'EA. Les modèles AI prim ont montré une précision prometteuse dans la prédiction de la décroissance de la résistance résiduelle avec la déformation, sur la base des modèles dans les enregistrements d'énergie AE.Les résultats indiquent que l'AE prééchec encapsule en effet des informations sur les mécanismes de défaillance en développement et la réponse postdéfaillance qui peut être capturé par l'intelligence artificielle.

KEYWORDS: Residual Strength, Acoustic Emission, Discrete Element Method, Artificial Intelligence, Long Short-Term Memory.

#### 1 INTRODUCTION.

Design of engineering structures supported by rock formations, such as tunnels and mines, relies heavily on accurate assessments of the strength characteristics of rock masses. The knowledge of rock mass behavior becomes also essential in other fields such as reservoir engineering, seismology, and plate tectonics. Such brittle materials are prone to multiple plausible modes of failure that are affected by their complex loading history as well as the presence of heterogeneous micro-cracks and joints (Lawn 1993; Rao et al. 2003). Moreover, the interplay between the mechanical properties and the spatial heterogeneity can lead to progressive failure mechanisms along the path of least resistance (Mortell, Tanner, and McCarthy 2016; Prudencio and Jan 2007; Yang, Xue, and Zhang 2018).

Such particularities in failure mechanisms justifiably necessities the design process to be complemented by appropriate ongoing monitoring methods that provides continuous feedback for reevaluating the analysis and design assumptions (Stanchits, Burghardt, and Surdi 2015). Given its accessibility, acoustic emission (AE) is an apt practical candidate for such a measure that can be easily recorded and tracked in situ, as well as in the laboratory and numerical simulations. The acoustic energy release can well indicate processes such as crack initiation, propagation, and failure in rocks (see Figure 1). Indeed, AE sensors have been widely used in a variety of laboratory tests and field measurements, to capture the progression of rock failure, see Feng et al. (2019) and the references therein for a complete review of the literature.

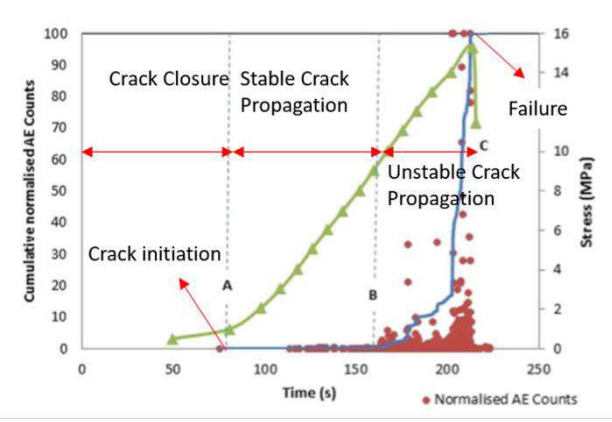


Figure 1. A stress and accumulative AE counts vs strain, from a unconfined compression test on a Brown Coal sample (Vishal, Ranjith, and Singh 2015).

The strong sensitivity of failure mechanisms and characteristics to the samples particularities seriously hinders an experimental parametric study (Xia et al. 2000). This, however, can be overcome by resorting to appropriate numerical simulations. In this regard, the Discrete Element Method (DEM) has been successfully adopted in recent years for numerical simulation of rocks. The original procedure developed for granular materials was further extended in Potyondy and Cundall (2004) where a rock medium is simulated as an assembly of tightly packed particles that are bonded to each other via cohesive interactions. The significant body of literature that followed have convincingly shown the DEM to be capable of capturing the salient mechanical aspects of rock and concrete media based on simple microscopic parameters such as

interparticle contact stiffness and bond strength (Jing and Stephansson 2007; Scholtès and Donzé 2012; Pouragha, Eghbalian, and Wan 2020).

DEM simulations are particularly useful for the study of AE since they provide access to microscale data that is often not easily accessible in experiments. Among such data, is the information about the bond breakage and the associated released energy in the form of acoustic emission. DEM has been recently adopted as a convenient and powerful tool to study the characteristics of AE events in rocks (and concrete) prior, during and after failure (Caulk 2020; Xie et al. 2020; Gao et al. 2019; Ma et al. 2020).

Following the discussion above, the current study aims at predicting the post-failure behavior, and in particular residual strength of rock formations based on their pre-failure behavior by using AE recordings in DEM simulations. The deep learning method using the Long short-term memory (LSTM) algorithm has been adopted in processing the data. The hypothesis here is whether pre-failure patterns in AE signal data can be correlated with the post-failure behaviour, i.e. the gradual decay of postpeak strength with strain. To generate diversity in the data, the inter-particle friction, which is activated after bond breakage, is varied over a range, while the inter-particle cohesive bond strength is kept constant across different samples. The AE data obtained from synthetic compression tests simulated through DEM is used to develop and validate the AI algorithms, establishing predictive relations between AE energy variation patterns and post-failure stress-strain behavior of rock samples.

#### 2 METHODOLOGY

#### 2.1 DEM Simulations

The open-source YADE software (Šmilauer et al. 2010) has been used in this study to carry out two dimensional DEM simulations on assemblies of circular particles with a uniform particle size distribution between  $r_{min}$  and  $r_{max}$  with  $r_{max}/r_{min} = 2.0$ . The elastic contact stiffness follows a linear model with the same stiffness along the normal and tangential directions, calculated as  $k = 2Er_1r_2/(r_1 + r_2)$  for a contact between two particles with radii of  $r_1$  and  $r_2$ , where E is a stiffness parameter. All the samples have 1-to-2 aspect ratios and are confined by frictionless rigid walls. The sample was first compacted under 2D confinement stress  $p_0 = 5 \text{ kN/m}$ considering the average particle size of 1 mm, is equivalent of 5 MPa in 3D. No interparticle friction or cohesion is considered in this stage to obtain a dense sample. After reaching the desired stress, the cohesive bonds are activated at all existing contact points. The strength of these bonds are the same along the tangential and tensile normal directions and is calculated as  $f_{\text{max}} = c \left( \min(r_1, r_2) \right)^2$ with the stress-like parameter c determining the bond strength. After a bond is broken, a Coulomb friction law is activated restricting the tangential force with the interparticle friction of  $\mu$ .

In these simulations, the dimensionless initial confining pressure is  $p_0/(E\bar{r}) = 5e - 2$  with  $\bar{r}$  being the average particle radius, and the dimensionless bond cohesion is c/E =2.17 e - 2. Considering that the behaviour of contacts after bond breakage is controlled by the interparticle friction, the value of  $\mu$  was varied between 0.01 and 0.5 to capture the effect of friction on the post-peak response. A total of 17 simulations were carried out: 10 simulations by starting from similar initial 10,000 arrangement of particles {0.01, 0.02, 0.03, 0.04, 0.05, 0.06, 0.07, 0.08, 0.09, 0.10}, and 7 simulations by starting from another initial arrangement of 20,000 particles and  $\{0.05, 0.10, 0.15, 0.20, 0.30, 0.40, 0.50\}.$ 

The biaxial quasi-static deviatoric compression loading was performed by applying a constant compressive strain rate to the top and bottom walls while the stress on the lateral walls were kept constant via a servo-control mechanism. Upon the breakage of a bond, the released elastic energy is measured as:

$$\Delta E = \frac{f_n^2}{2k_n} + \frac{f_t^2}{2k_t} \tag{1}$$

where  $\Delta E$  is the released energy due to the breakage of the bond with stiffness of  $k_n$  and  $k_t$  along the normal and tangential directions (which are the same for our simulations), and  $f_n$  and  $f_t$  are the normal and tangential components of the contact force prior to the bond breakage. The total elastic energy released was calculated by accumulating the energy of broken bonds during intervals of the axial strain.

## 2.2 Biaxial Compression and AE Test Data

Figure 2 presents the stress-strain and AE evolution for various values of interparticle friction,  $\mu$ . Both peak and residual strength values increase for larger  $\mu$ . While the simulations were run up to an axial strain of 25%, only the results for the first 2.5% of axial strain has been used for training and validation of the AI algorithms, as the residual strength remains relatively stationary after this strain level. The two sets of data from DEM simulations, i.e. stress-strain and records of AE events versus strain were merged based on the strain intervals where AE events were captured. The "AE counts" reflects AE event counts (bond breakage) per unit volume at each strain interval which scales linearly with AE energy.

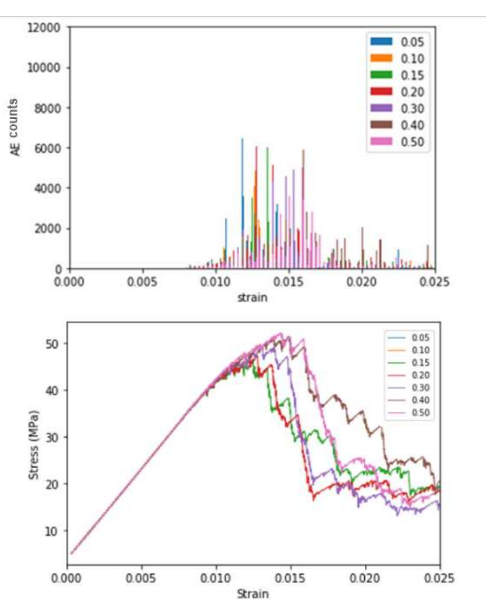


Figure 2. Example of DEM simulation data. (top) AE counts vs axial strain, (bottom) axial stress vs axial strain

## 2.3 Deep Learning Using LSTMs

LSTM networks were developed in this study to forecast the trends of post-failure stress-strain variation based on pre-failure AE data. LSTM networks belong to the broader class of Recurrent Neural Networks (RNNs) with special internal memory units that can be updated, erased or read out (Hochreiter and Schmidhuber 1997; Ordóñez and Roggen 2016).

These networks have proven particularly successful for recognizing temporal patterns in time-series data. In addition to feed-forward connections, computational units (neurons), RNNs have recurrent connections where the output of a unit is fed back to itself with a weight and a time delay, which provides the algorithm with a memory of past activations. Stacking memory units in such networks enables learning higher levels of temporal

patterns in sequential data. LSTMs have been successfully applied in stock market forecast, as well as in text, language and voice recognition (Ray, Rajeswar, and Chaudhury 2015). LSTMs have been also recently used in forecast applications in infrastructure and geotechnical engineering (Yousefpour et al. 2021). Figure 3 provides a diagram of the developed LSTM architecture in this study.

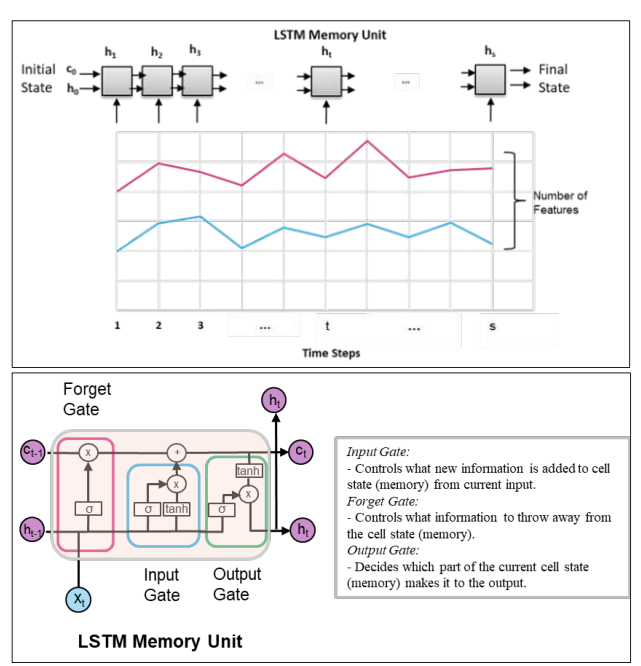


Figure 3. LSTM network architecture; (top) LSTM unit unfolded in time, (bottom) LSTM memory unit and gates.

## 2.3.1 LSTM Model Configuration

A grid search was performed to find the best configurations of the LSTM algorithm and the optimum values of the hyperparameters. The hyperparameters include the number of LSTM units, number of hidden neurons, optimization algorithm, initial gradient decay rate, maximum number of epochs, training and test data size, and number of sequences (sequence length). The range of values tested for each hyperparameter and the selected values are given in Table 1.

# 2.3.2 Data Partitioning

Various data partitioning methods were experimented to ensure models were properly trained. The division that best captured the pre-failure in training and post-failure in validation/testing was found to be 80, 15, 5% for training, testing and validation, respectively. The performance of LSTM models during training was monitored based on the validation dataset; training stopped when error over the validation dataset consistently increased for a certain number of epochs (stopping criteria). The test dataset was used to evaluate the overall performance of the models for unseen data. Figure 4 shows an example of data partitioning. Note that the data has been normalized before training.

Table 1. LSTM hyperparameters.

**************************************		
Parameter	Tested Range	Selected Value
# of LSTM Units	1,2	1
# of Hidden Neurons	32, 64, 128	64
Initial Gradient Decay Rate	0.01, 0.005, 0.001	0.005
Dropout Ratio	0. 0.2	Variable

Input-Label Length

20,5; 20,10; 30,10; 40,30; 50,5; 50,10; 50,20; 80,20; 80,30; 80,60; 100,50

Variable

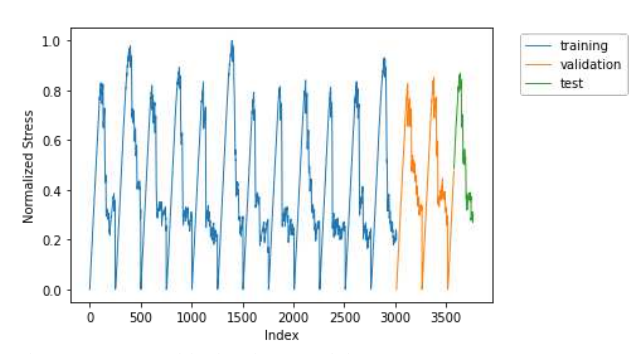


Figure 4. Data partitioning for AI training.

#### 2.3.3 Training and Data Slicing

To train the LSTMs, data first needs to be sliced into smaller sequences through a sliding window. In each slice, a certain number of time steps are treated as input (input length) to the network while a number of time-steps into the future are predicted (label). The total sequence length is the sum of the two time-steps (see Figure 5).

Single-Shot (ssh) and Feedback (fb) methods were considered herein for training the LSTMs. In single-shot training, all the time-steps were predicted at once, as shown in Figure 6. In this example, the model predicts the next 24 steps based on the same time-span input. In the Feedback method, instead of the actual reading, the prediction at each time-step is input in the next time-step.

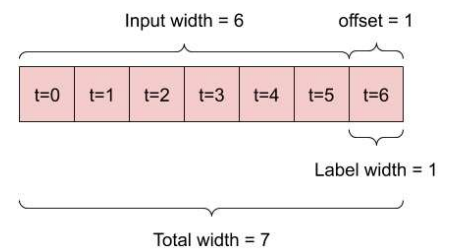


Figure 5. Definition of input and label in data slicing.

#### 2.3.4 Feature Selection

As presented in Table 2, four combinations of features have been considered to compare the performance of the AI models under various scenarios. The most challenging, and most practically valuable scenario is when the pre-failure strain-stress is not available and the only available input feature is the AE readings. Also, the scenarios without AE as input were analysed to better understand the impacts of AE on post-failure patterns recognition by AI. The strain intervals in the data were gradually increasing towards the failure point to keep up with the increase in the rate of AE events around the stress peak, therefore the significance of including strain as an input feature was also evaluated.

Table 2. LSTM Input Features

uote 2. E5 111 input i cutures			
Parameter	Tested Range	Abbreviation	
Input Features	[strain, stress, AE],	[SSAE],	
	[strain, stress],	[SS],	
	[stress],	[S],	
	[AE]	[AE]	

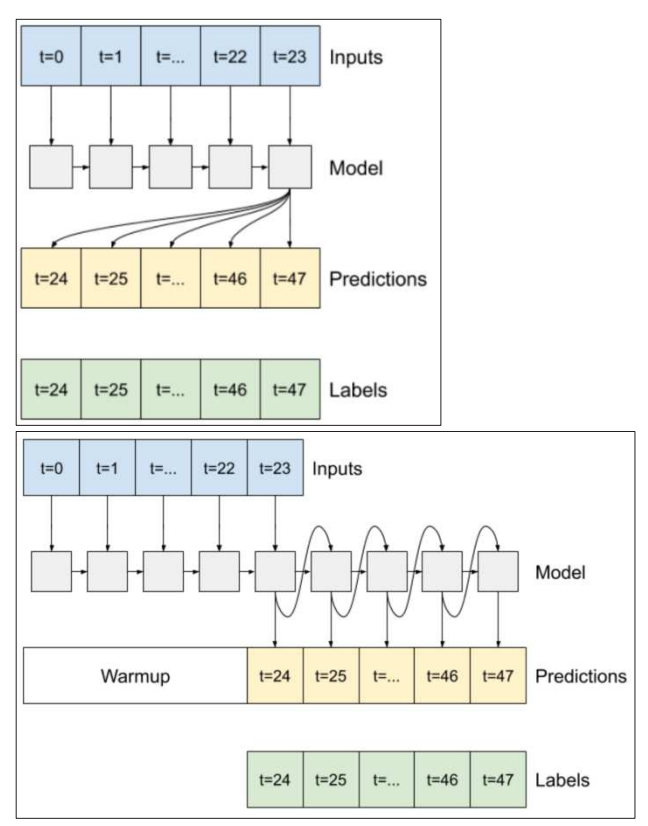


Figure 6. LSTM Training Methods (Google 2020); (top) Single Shot, (bottom) Feedback.

#### 3 RESULTS AND DISCUSSIONS

## 3.1 Grid Search and LSTM Configurations

The key results from grid search analyses are compiled in Figure 7. The name of each LSTM configuration follows the following pattern: "Feature Combination - Training Method - (Input, Label) - No. of Hidden Units - Drop Out". The performance measurement metric was the mean absolute error (MAE) of predictions over the label length. Among various factors, the input-label (slice) length showed the most significant impact on the LSTM performance, followed by the training method and the number of the LSTM units. For each feature combination, the optimum input-label length was identified; for models including all three features, increasing the input length to 80 significantly improved the prediction power, whereas increasing the input length from 20 to 50 resulted in only slight improvements. A similar trend was observed for the other models involving stress-strain features. For the models with AE as the only input feature, MAE showed a declining trend with the input length, reaching its minimum range at 50. Increasing the input length to 80 and then 100 significantly reduced the prediction accuracy

Single Shot training method showed to slightly outperform the Feedback method, although this pattern was not found in all the feature combinations. Increasing the LSTM units from one to two, did not result in significant performance improvements. Also, the optimum number of hidden neurons was found at 64. Adding a dropout of 20% during training, showed to increase the variability in MAE within the reputations, but the mean value did not show a decreasing trend.

#### 3.2 AI Predictions

The post-failure predictions for various feature combinations are compared in Figure 8 for the input-label length = (80,60). Feature combinations including stress [SSAE, SS, S] show much greater accuracy in predictions compared to [AE]. This trend indicates the insignificant impacts of AE when strain-stress trend is

available as an input feature. However, the AI model with only AE as the input feature can still predict the post-failure stress-strain trends, with reasonably accuracy. Figure 9 shows how maneuvering around input-label length can improve the performance of the AI models and that even with AE alone a significantly improved accuracy can be achieved at the optimum input-label length [(50,10)].

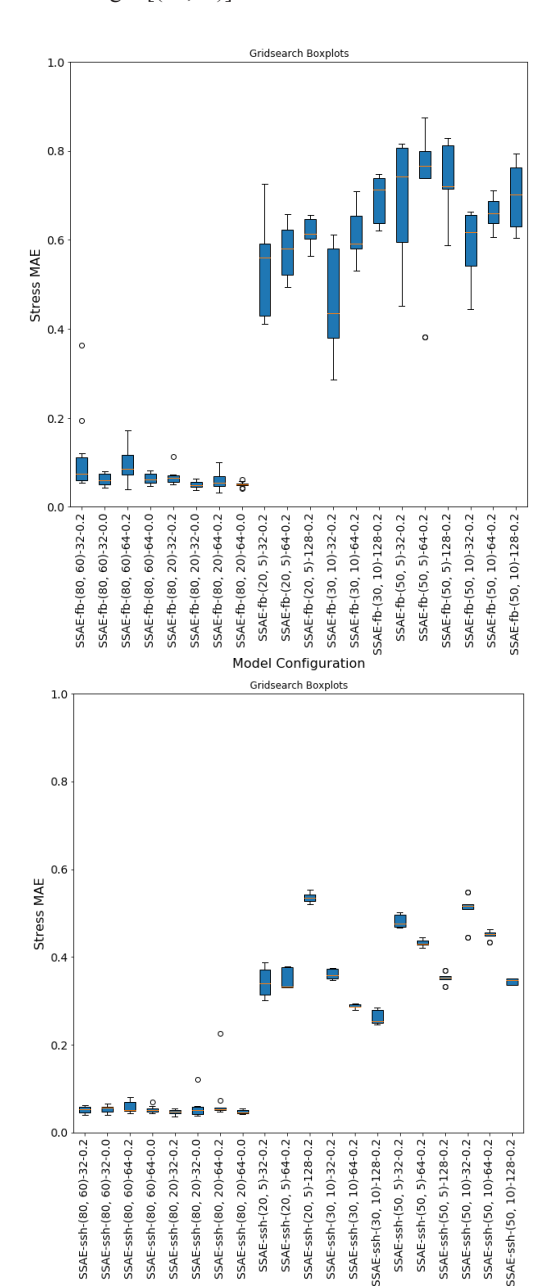


Figure 7. The performance of LSTM configurations, features= [SSAE], (top) Feedback, (bottom): Singleshot.

Model Configuration

# 4 CONCLUSIONS

This study introduces an innovative AI approach to predict the post-failure behaviour and residual strength of rocks based on the pre-failure patterns of AE energy. LSTM algorithms were implemented and properly trained using data generated through DEM simulations of rock under biaxial compression loading. A total of 17 DEM simulations were considered with varying interparticle friction values and constant interparticle bond cohesion. The results indicate that patterns of AE events prior to failure indeed contain valuable information about the emerging failure mechanisms leading to the post-failure decay in rocks,

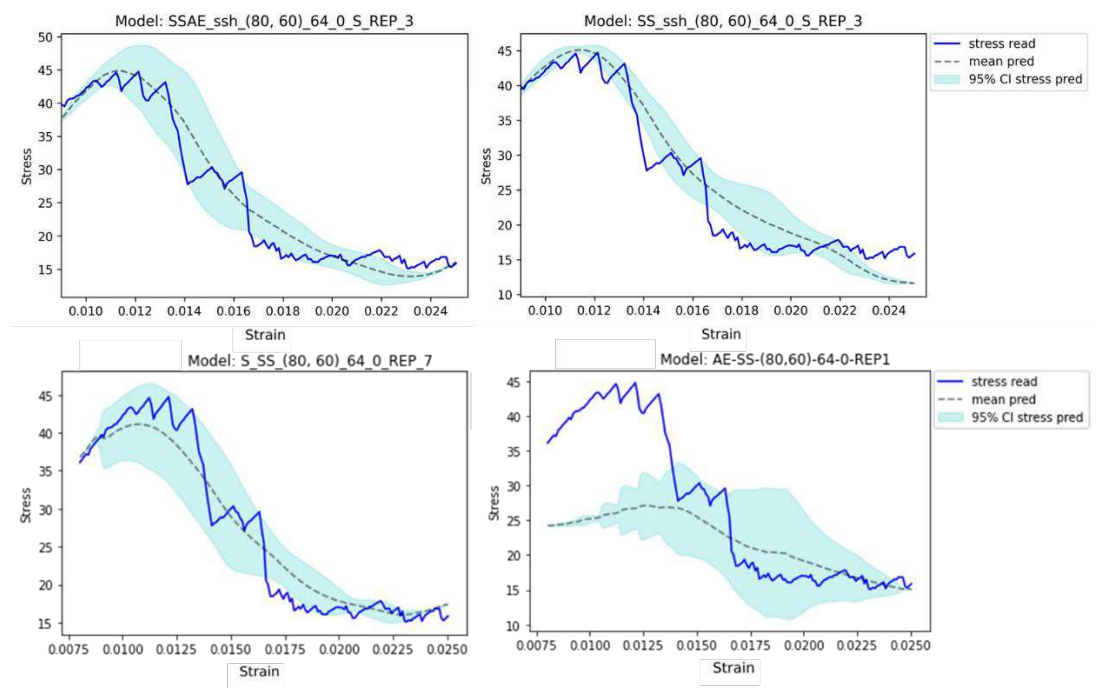


Figure 8. Post-failure predictions by the AI models for different input feature combinations over selected test samples; in order from top left to bottom right: [SSAE], [SS], [S], [AE]; mu= 0.12

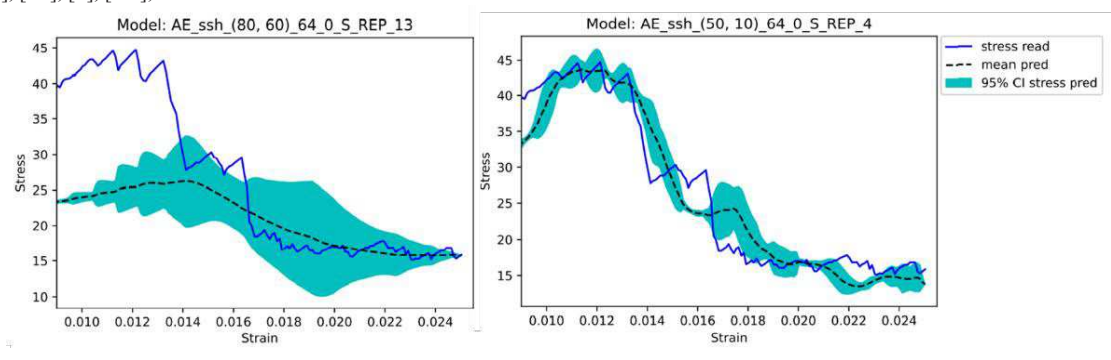


Figure 9. Impact of slicing length on the post-failure predictions: (80,60) [left] and (50,10) [right]; Features=[AE] and mu=0.12

and that LSTM algorithms can capture these complex correlations. Given the significance of the residual strength as a design parameter, this research puts forward a novel method to provide more reliable, dynamic estimates, by combining AE sensors and AI technology. The outcome shows the remarkable potential of deep learning methods for capturing complex patterns in the response of heterogeneous geo-materials.

# 5 REFERENCES

Caulk, Robert A. 2020. "Modeling Acoustic Emissions in Heterogeneous Rocks during Tensile Fracture with the Discrete Element Method." Open Geomechanics 2.

Feng, Xia-Ting, R P Young, J M Reyes-Montes, Ömer Aydan, Tsuyoshi Ishida, Jian-Po Liu, and Hua-Ji Liu. 2019. "ISRM Suggested Method for in Situ Acoustic Emission Monitoring of the Fracturing Process in Rock Masses." *Rock Mechanics and Rock Engineering* 52 (5): 1395–1414.

Gao, Ke, Robert Guyer, Esteban Rougier, Christopher X Ren, and Paul A Johnson. 2019. "From Stress Chains to Acoustic Emission." Physical Review Letters 123 (4): 48003.

Google. 2020. "Time Series Forecasting."

https://www.tensorflow.org/tutorials/structured\_data/time\_series.

Hochreiter, Sepp, and Jürgen Schmidhuber. 1997. "Long Short-Term Memory." Neural Computation 9 (8): 1735–80.

Jing, Lanru, and Ove Stephansson. 2007. Fundamentals of Discrete Element Methods for Rock Engineering: Theory and Applications. Vol. 85. Elsevier.

Lawn, Brian. 1993. Fracture of Brittle Solids. Cambridge university

press.

Ma, Jun, Shunchuan Wu, Xiao-Ping Zhang, and Yixiang Gan. 2020. "Modeling Acoustic Emission in the Brazilian Test Using Moment Tensor Inversion." Computers and Geotechnics 123: 103567.

Mortell, Daniel J, David A Tanner, and Conor T McCarthy. 2016. "An Experimental Investigation into Multi-Scale Damage Progression in Laminated Composites in Bending." *Composite Structures* 149: 33–40

Ordóñez, Francisco Javier, and Daniel Roggen. 2016. "Deep Convolutional and Lstm Recurrent Neural Networks for Multimodal Wearable Activity Recognition." *Sensors* 16 (1): 115.

Potyondy, David O, and P A Cundall. 2004. "A Bonded-Particle Model for Rock." *International Journal of Rock Mechanics and Mining Sciences* 41 (8): 1329–64.

Pouragha, Mehdi, Mahdad Eghbalian, and Richard Wan. 2020. "Micromechanical Correlation between Elasticity and Strength Characteristics of Anisotropic Rocks." *International Journal of Rock Mechanics and Mining Sciences* 125: 104154.

Prudencio, M, and M Van Sint Jan. 2007. "Strength and Failure Modes of Rock Mass Models with Non-Persistent Joints." *International Journal of Rock Mechanics and Mining Sciences* 44 (6): 890–902.

Rao, Qiuhua, Zongqi Sun, Ove Stephansson, Chunlin Li, and Bengt Stillborg. 2003. "Shear Fracture (Mode II) of Brittle Rock." International Journal of Rock Mechanics and Mining Sciences 40 (3): 355–75.

Ray, Anupama, Sai Rajeswar, and Santanu Chaudhury. 2015. "Text Recognition Using Deep BLSTM Networks." In 2015 Eighth International Conference on Advances in Pattern Recognition (ICAPR), 1–6. https://doi.org/10.1109/ICAPR.2015.7050699.

- Scholtès, L U C, and Frédéric-Victor Donzé. 2012. "Modelling Progressive Failure in Fractured Rock Masses Using a 3D Discrete Element Method." *International Journal of Rock Mechanics and Mining Sciences* 52: 18–30.
- Šmilauer, Václav, Emanuele Catalano, Bruno Chareyre, Sergei Dorofeenko, Jerome Duriez, Anton Gladky, Janek Kozicki, et al. 2010. "Yade Reference Documentation." Yade Documentation 474: 1–531.
- Stanchits, Sergey, Jeffrey Burghardt, and Aniket Surdi. 2015. "Hydraulic Fracturing of Heterogeneous Rock Monitored by Acoustic Emission." *Rock Mechanics and Rock Engineering* 48 (6): 2513–27.
- Xia, Mengfen, Fujiu Ke, Yujie Wei, Jie Bai, and Yilong Bai. 2000. "Evolution Induced Catastrophe in a Nonlinear Dynamical Model of Material Failure." Nonlinear Dynamics 22 (2): 195–214.
- Xie, Chao, Linjuan Yuan, Min Zhao, and Yinghui Jia. 2020. "Study on Failure Mechanism of Porous Concrete Based on Acoustic Emission and Discrete Element Method." Construction and Building Materials 235: 117409.
- Yang, Baicun, Lei Xue, and Ke Zhang. 2018. "X-Ray Micro-Computed Tomography Study of the Propagation of Cracks in Shale during Uniaxial Compression." Environmental Earth Sciences 77 (18): 1–9.
- Yousefpour, Negin, Steve Downie, Steve Walker, Nathan Perkins, and Hristo Dikanski. 2021. "Machine Learning Solutions for Bridge Scour Forecast Based on Monitoring Data." *Transportation Research Record*, 03611981211012693.